Chinese Physics B

PAPER

High harmonic generation in crystal SiO_2 by sub-10-fs laser pulses

To cite this article: Shuai Wang *et al* 2023 *Chinese Phys. B* **32** 063301

High harmonic generation in crystal SiO_2 by sub-10-fs laser pulses

Shuai Wang(王帅)[1,2], Jiawei Guo(郭嘉为)[4], Xinkui He(贺新奎)[1,2,3,†], Yueying Liang(梁玥瑛)[1,2], Baichuan Xie(谢百川)[1,2], Shiyang Zhong(钟诗阳)[1], Hao Teng(滕浩)[1], and Zhiyi Wei(魏志义)[1,2,3,‡]

[1] *Beijing National Laboratory for Condensed Matter Physics, Institute of Physics, Chinese Academy of Sciences, Beijing* 100190, *China*
[2] *University of Chinese Academy of Sciences, Beijing* 100490, *China*
[3] *Songshan Lake Materials Laboratory, Dongguan* 523808, *China*
[4] *School of Physics, Nankai University, Tianjin* 300071, *China*

(Received 22 February 2023; revised manuscript received 10 March 2023; accepted manuscript online 15 March 2023)

The high harmonic generation (HHG) by few-cycle laser pulses is essential for research in strong-field solid-state physics. Through comparison of high harmonic spectra of solids generated by laser pulses with varying durations, we discovered that lasers with good dispersion compensation are capable of producing a broad spectrum of high harmonics. As the pulse duration is further compressed, several interference peaks appear in the broad spectrum. Moreover, we conducted simulations using the semiconductor Bloch equation, considering the effect of Berry curvature, to better understand this process. Our work provides a valuable approach for studying HHG by few-cycle laser pulses in solid materials, expanding the application of HHG in attosecond physics.

Keywords: solid state hhg, few-cycle laser pulses, broad spectrum, interference peak

PACS: 33.20.Xx **DOI:** 10.1088/1674-1056/acc452

1. Introduction

High-order harmonics generated in a gas medium, as a coherent laser source with high photon energy, has been developed for over 20 years and was widely used in high-harmonic spectroscopy, attosecond generation, and ultrafast dynamic.[1–7] In recent years, with the femtosecond laser producing high harmonics in crystal ZnO for the first time,[8] the exploration of high harmonics in solids has gradually become a research focus. Despite successful observations of HHG in a variety of solid media,[9–17] the physical picture of HHG in solids is still under discussion. As a common approach, HHG in solids can be described with two dynamical behaviors, called interband and intraband radiation.[18–25] Interband radiation arises from the recombination of electrons and holes between the conduction and valence bands, while intraband radiation arises from Bloch oscillations of electrons and holes within the band. The first step is to excite electrons from the valence band to the conduction band, which requires that the photon energy of driven laser is less than the minimum band gap of the material.

Mid-infrared lasers with low photon energy are typically used to drive HHG in narrow band gap materials such as ZnO,[8,26] GaSe,[12,27] MoS_2,[9] and graphene.[14,28] For the material SiO_2 with a bandgap of 9 eV, it can be driven by mid-infrared laser[17] or near-infrared laser.[29] Previous experiments using long-pulse near-infrared lasers to drive crystal SiO_2 produced high harmonics of both odd and even order.[29] The appearance of even harmonics in the vertical direction was caused by the reversal symmetry breakdown in crystal SiO_2. Experiments with amorphous and crystal SiO_2 were conducted using fewcycle mid-infrared lasers to explore the role of long-range order in HHG,[17] and it was found that HHG in crystal SiO_2 produced a broad spectrum. Therefore, we ask whether a similar phenomenon can occur when a near-infrared fewcycle laser is used to drive crystal SiO_2?

Based on this, we conducted an experiment on HHG driven by a near-infrared few-cycle laser, comparing the information obtained from HHG driven by lasers with different pulse durations. Multiple interference peaks were observed at the shortest pulse duration, and the frequencies corresponding to these interference peaks were studied at different laser field intensities.

2. Experimental details

The experimental setup is illustrated in Fig. 1. A Ti:sapphire laser was used as the front-end source, with a pulse duration of 35 fs, pulse energy of 7 mJ, and beam diameter of 13 mm at a repetition rate of 1 kHz. To couple the laser beam into a 0.9-m long, 400-μm diameter optical fiber, a concave focusing mirror (CM1) with a focal length of 2.5 m was employed. The hollow fiber was placed in a U-shaped groove, integrated into a 40 mm diameter vacuum pipe with optical windows made of fused quartz at both ends. The windows were oriented at a Brewster's angle to minimize reflection losses, and coated with an anti-reflection layer (450 nm–1000 nm) to further reduce reflections. The wide spectrum laser emerging

†Corresponding author. E-mail: xinkuihe@iphy.ac.cn
‡Corresponding author. E-mail: zywei@iphy.ac.cn

from the rear window was astigmatic, and was collimated by a silver-plated mirror with a focal length of 2 m. The collimated laser was then passed through a pair of chirped mirrors, with a pair of parallel wedges introduced to ensure accurate second-order dispersion control. This allowed us to obtain the shortest possible pulse output.

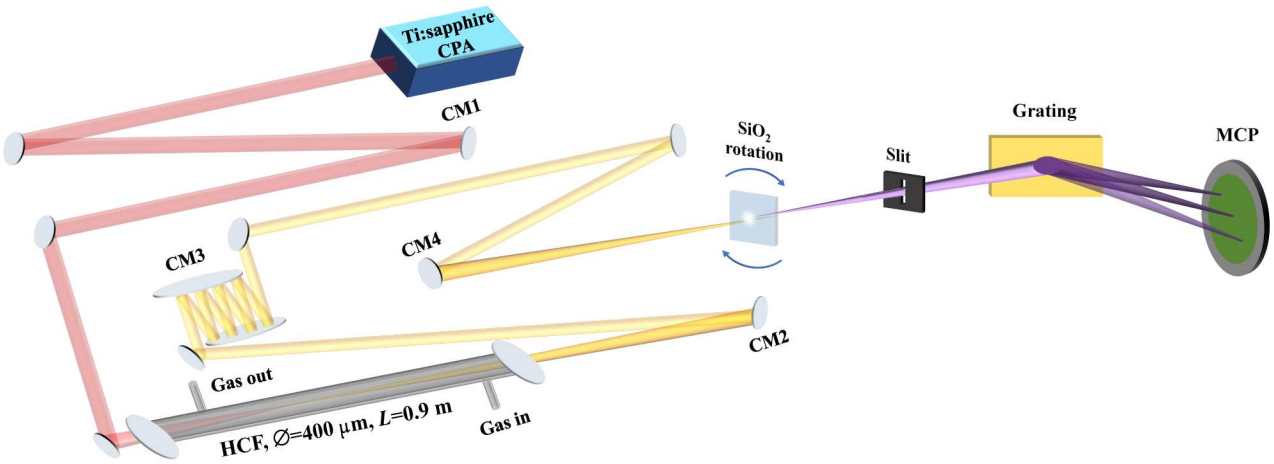

Fig. 1. Schematic diagram of experimental set up. CM1–2: curved mirror with focal length $f_1 = 2.5$ m and $f_2 = 2$ m; CM3: chirped mirrors; CM4: curved mirror with focal length $f_4 = 1.3$ m.

In the experiment, the drive laser energy was adjusted by electric diaphragm with the adjustable accuracy of 0.1 mm. The laser beam was then focused onto a z-cut crystal SiO_2 through a concave mirror with a focal length of 1.3 m. To facilitate precise measurements, the crystal SiO_2 could be rotated with a precision of 0.05°. The high harmonic generation from the solid target was then propagated to a self-developed spectrometer for measurement. This spectrometer consisted of a slit, a flat-field grating, and a microchannel plate (MCP). The resolution of the spectrometer can be improved by adjusting the slit width. The spatial frequency distribution of HHG can be displayed on MCP and recorded by CCD. Since solids typically generate low-order harmonics, an XUV grating with 600/mm was used for this experiment, and the flat-field spectrum covered a range of 22 nm–124 nm.

3. Results and discussion

The transmittance of the laser pulse is nearly 74% when the energy of the input pulse is 1.7 mJ and the output pulse energy is 1.25 mJ. After chirped mirror and wedge compression, the remaining pulse energy is 1 mJ. D-scan measurement is used to determine the shortest pulse duration of 5.59 fs and the central wavelength of 750 nm when the input pressure is 1.6 bar (1 bar $= 10^5$ Pa), as shown in Fig. 2(a). When the input pressure is 0.5 bar, the pulse duration is 10.36 fs and the central wavelength is 795.3 nm, as shown in Fig. 2(b). The figure shows that when the air pressure is 0.5 bar, the phase of the spectrum is flat, and the compression system can compensate for the phase to obtain a pulse duration close to the Fourier transform limit. However, when the pressure is increased to 1.6 bar, the pulse spectrum covers a wider range of 500 nm–1000 nm, and the third-order dispersion of the wide spectrum cannot be compensated. As a result, a small pulse appears next to the main pulse, and the peak intensity of the small pulse is $1/3$ of the peak intensity of the main pulse.

The high-order harmonics obtained are presented in Figs. 2(c) and 2(d). The upper part of each figure shows the spatial frequency distribution of the high-order harmonics, while the lower part shows the spectra obtained by integrating the spatial axis. The energy range of the HHG obtained using the two different few-cycle pulses is consistent and extends up to 20 eV. However, when the laser pulse duration is 10.36 fs, two flat spectra are produced, one with a wide spectrum range of 14 eV–20 eV and the other with a spectrum range of 10 eV–12 eV. The two segments of the spectrum are separated by one photon energy (1.65 eV). This is due to the presence of both odd and even harmonics in the crystal SiO_2, which produces a more continuous pattern when driven by few-cycle pulses with a wide spectrum. When the laser pulse duration is 5.59 fs, five interference peaks appear in the previous spectrum of 14 eV–18 eV, and the corresponding harmonic photon energies of these five peaks are 13.98 eV, 14.73 eV, 15.54 eV, 16.17 eV, and 16.95 eV, respectively. They are approximately 9, 9.5, 10, 10.5, and 11 times the photon energy of the laser with a central wavelength of 800 nm (1.55 eV), and there is no integer or half-integer multiple relationship between them and the photon energy of the laser with a central wavelength of 750 nm (1.65 eV).

To further analyze this result, the laser pulse duration was held at 5.59 fs, and the change in photon energy corresponding to the five peaks with laser field intensity was measured, as shown in Fig. 3. When the laser power density is 1.92×10^{12} W/cm^2, the first interference peak does not appear, but the remaining four interference peaks do. As the

laser power density increases further until the crystal is damaged, the five interference peaks always exist, and the photon frequency corresponding to the interference peaks remains mostly unchanged. This may be the result of the interference between the HHG produced by the small pulse and the HHG produced by the main pulse.

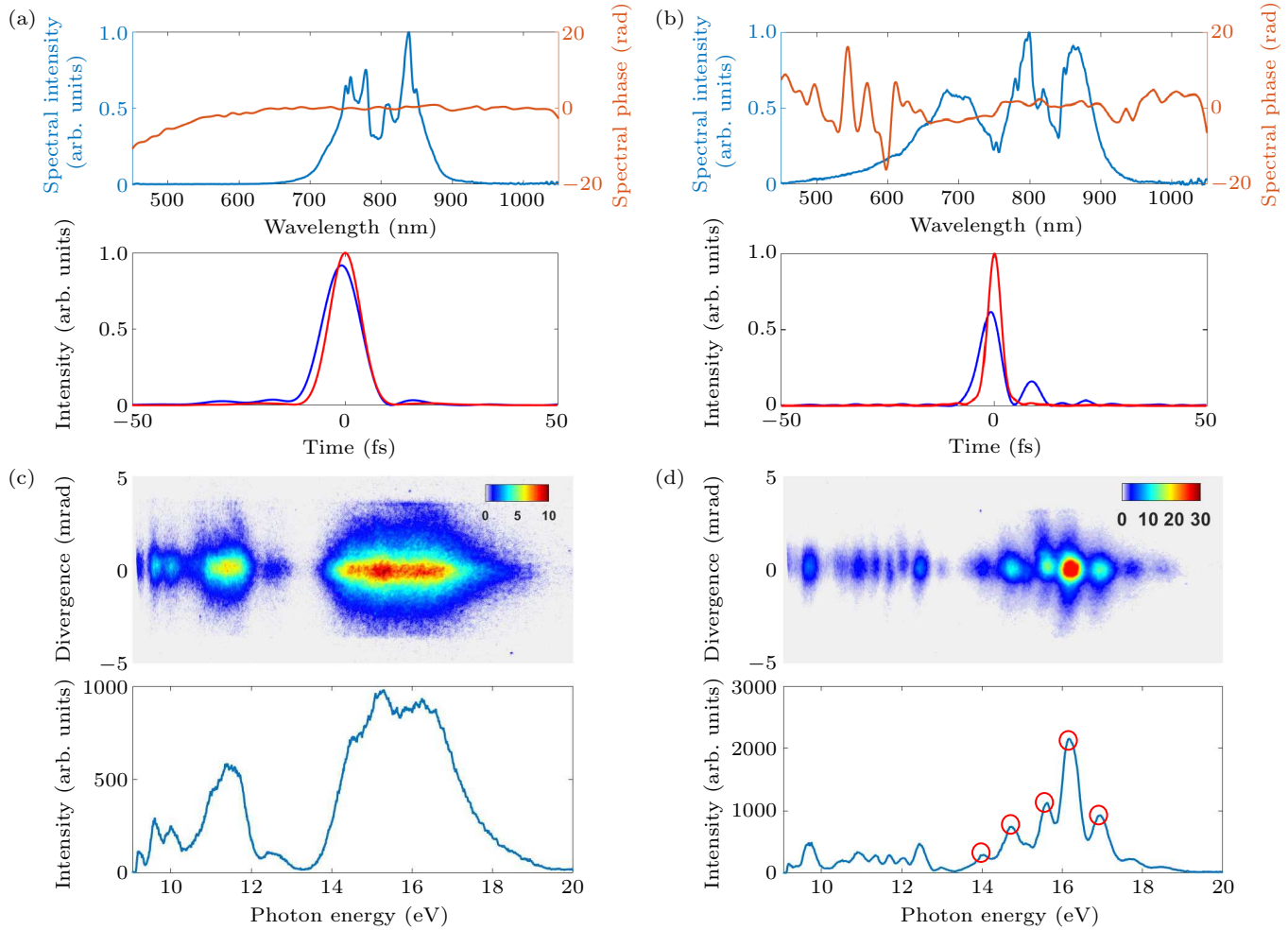

Fig. 2. (a) The upper figure shows the laser spectrum (blue solid line) and the corresponding phase of the spectrum (yellow solid line). The lower figure shows the temporal pulse shape of 10.36 fs (red line) together with the transform-limited shape (blue line). (b) The upper figure shows the laser spectrum (blue solid line) and the corresponding phase of the spectrum (yellow solid line). The lower figure shows the temporal pulse shape of 5.59 fs (blue line) together with the transform-limited shape (red line). (c) Measured high harmonics in crystal SiO_2 (100 μm) with the input laser energy of 220 mW and laser pulse duration of 10.36 fs. (d) Measured high harmonics in crystal SiO_2 (100 nm) with the input laser energy of 230 mW and laser pulse duration of 5.59 fs.

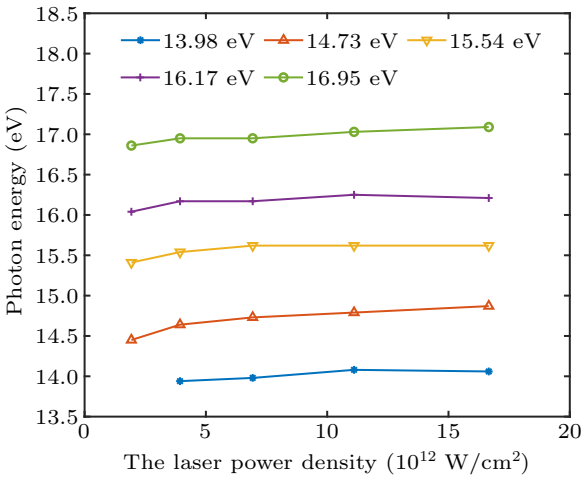

Fig. 3. Measured photon energy corresponding to the five peaks with the different laser field intensities.

In order to investigate the physical mechanism of the HHG using the main pulse and the small pulse, the semiconductor Bloch equations (SBE) are used for simulating the high harmonic generation in SiO_2. The two-band model reads

$$\frac{\partial \pi(K,t)}{\partial t} = -\frac{\pi(K,t)}{T_2} - \mathrm{i}\xi(K,t)[n_\mathrm{v} - n_\mathrm{c}]\,\mathrm{e}^{-\mathrm{i}S(K,t)}, \quad (1)$$

$$\frac{\partial n_\mathrm{v}(K,t)}{\partial t} = -\mathrm{i}\xi^*(K,t)\pi(K,t)\,\mathrm{e}^{\mathrm{i}S(K,t)}, \quad (2)$$

$$\frac{\partial n_\mathrm{v}(K,t) + n_\mathrm{c}(K,t)}{\partial t} = 0, \quad (3)$$

where n_m ($m = \mathrm{c},\ \mathrm{v}$) is the population of the conduction band and valence band, $S(K,t) = \int_{t_0}^{t'}(\varepsilon_\mathrm{g}(K + A(\tau)))\mathrm{d}\tau$ is the classical action and $\varepsilon_\mathrm{g} = E_\mathrm{c} - E_\mathrm{v}$ is the bandgap. $\xi^*(K,t) = F(t)\,\mathrm{d}(K + A(t))$ is the Rabi frequency, and $d(k) = \mathrm{i}\int \mathrm{d}^3 x u^*_{\mathrm{v},k}(x)\nabla_k u_{\mathrm{c},k}(x)$ is the transition dipole moment, with $u_{m,k}(x)$ the periodic part of the Bloch function. We neglect the k dependence of the dipole moment. Moreover, d is set to be

3.46, which is the numerical value of the dipole moment at the Γ point. $K = k - A(t)$ is the shifted crystal momentum with the vector potential $A(t) = -\int F(t)\,\mathrm{d}t$, and the first Brillouin zone is also shifted to $\overline{BZ} = BZ - A(t)$. $T_2 = T_0/2$ is the dephasing-time term describing the coherence between the valence and conduction bands.

The harmonic generation process is dominated by the intraband radiation in crystal SiO_2. Thus, the population and the velocity of electron–hole pair affect the HHG according to

$$J_{\mathrm{ra}} = \sum_{m=\mathrm{c,v}} \int_{\overline{BZ}} v_m\left[K + A(t)\right] n_m(K,t)\,\mathrm{d}^3K. \tag{4}$$

To involve the even harmonics in the simulation, the effect of the Berry curvature in the velocity of electron–hole pair can be added independently. The velocity is calculated as

$$V_m\left(K + A(t)\right) = \frac{\partial \varepsilon_m[K + A(t)]}{\partial K} + \dot{F} \times \Omega_m[K + A(t)]. \tag{5}$$

For a more quantitative analysis, based on broken inversion symmetry features in momentum space, berry curvature and band dispersion can be represented by a series of spatial harmonics along the Γ–M direction[29]

$$\Omega_m(k) = \sum_{n=0}^{n_{\max}} \Omega_{m,n} \sin(nka), \tag{6}$$

$$\varepsilon_m(k) = \sum_{n=0}^{n_{\max}} \varepsilon_{m,n} \cos(nka). \tag{7}$$

Here, a is the lattice constant, $\Omega_{m,n}$ and $\varepsilon_{m,n}$ are the n-th Fourier coefficient of the berry curvature and the band m, respectively. To simplify the simulation, we use the maximum amplitude of the Fourier coefficients of band dispersion and curvature: $|\varepsilon_{m,n}|\,na = F_0|\Omega_{m,n}|$.

Since the electric field is linearly polarized along the $\hat{x} \| \Gamma$–M direction of the Brillouin zone, the laser field of two pulses is defined by

$$\begin{aligned} F(t) = \hat{x}\Big[& F_1\,\mathrm{e}^{-2\ln 2(t/\tau_{\mathrm{p1}})^2}\cos(\omega t) \\ & + F_2\,\mathrm{e}^{-2\ln 2((t-\tau)/\tau_{\mathrm{p2}})^2}\cos(\omega(t-\tau))\Big]. \end{aligned} \tag{8}$$

Here, ω is the frequency of the 750-nm laser, and $\tau = 9.84$ fs is the time delay between the two pulses. $\tau_{\mathrm{p1}} = 5.6$ fs is the pulse width of the main pulse, $\tau_{\mathrm{p2}} = 4.2$ fs is the pulse width of the small pulse. F_1 and F_2 represent the amplitudes of the main and small pulses, and the peak power of the main pulse is required to be three times the peak power of the small pulse, which is $F_1^2/F_2^2 = 3$. Total laser power density satisfies the condition, which is $I = F_0^2 = F_1^2 + F_2^2$. All parameters are set to be the same as experiment for comparison.

In the simulation, the total power density ranges from 5×10^{12} W/cm^2–14×10^{12} W/cm^2. Figure 4 shows the interference peaks in the spectral range of 14 eV–17 eV, which do not disappear as the laser intensity increases. Photon energies corresponding to the interference peaks are 14.35 eV, 14.72 eV, 15.08 eV, 15.64 eV, 16.03 eV, 16.39 eV, and 16.74 eV, respectively. Compared to the five different peaks obtained experimentally, seven different peaks were obtained theoretically. Theoretical simulations showed seven interference peaks in the spectral range of 14 eV–17 eV, while only five peaks were experimentally observed. The photon energies corresponding to the theoretically obtained interference peaks did not match the experimental results. This discrepancy is because the simulations only accounted for the spectral influence of the central wavelength when the two pulses interact with the material, ignoring the effect of other spectral components. The photon energies corresponding to different interference peaks are basically unchanged with the increase of laser power density, which is consistent with the experimental conclusion. It is shown that a coherent superposition of HHG by the small pulse and the main pulse leads to the interference peak on the broad spectrum. With the increase of laser power density, the corresponding frequency of the interference peak remains unchanged, indicating that the phase difference between the HHG by the two pulses is independent of the laser power density. As the laser power density increases, the distance between the interference peaks remains constant. Importantly, by analyzing the distance between the interference peaks, one can determine the time delay between the main pulse and the small pulses, which is crucial for reconstructing the temporal shape of the driving laser.

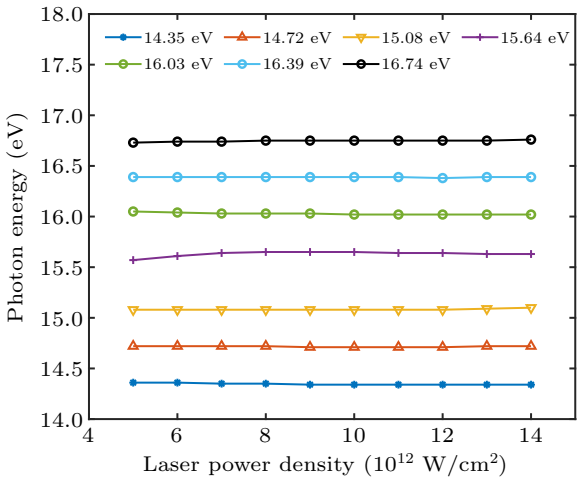

Fig. 4. Simulated photon energy corresponding to the seven peaks with the different laser field intensities.

4. Conclusion and perspectives

In conclusion, we have successfully generated high harmonics in a z-cut SiO_2 crystal with a thickness of 100 μm using few-cycle laser pulses in both experiment and theory. A single main pulse with a pulse duration of 10.36 fs was used to generate a broad spectrum of high harmonics. When the laser

duration was further compressed to 5.59 fs, a small pulse appeared next to the main pulse in the time domain, which led to the interference peak on the broad spectrum of high harmonics. We simulated the interference peaks of a broad spectrum caused by the coherent superposition of HHG by two pulses using the SBE, considering the effect of the Berry curvature. It was found that the photon energies corresponding to the interference peaks did not change with the laser power density. Our work also shows that the broad spectrum of high harmonics can be obtained only by using few-cycle laser pulses with good dispersion compensation. These results demonstrate the potential for using few-cycle laser pulses to efficiently generate high harmonics in solids, paving the way for the development of attosecond sources.

Acknowledgments

We thank the helpful discussions with Xiaoxing Zhou and Bingbing Wang. Project supported by the National Natural Science Foundation of China (Grant Nos. 91850209 and 11974416).

References

[1] Goulielmakis E, Yakovlev V S, Cavalieri A L, Uiberacker M, Pervak V, Apolonski A, Kienberger R, Kleineberg U and Krausz F 2007 *Science* **317** 769

[2] Hentschel M, Kienberger R, Spielmann C, Reider G A, Milosevic N, Brabec T, Corkum P, Heinzmann U, Drescher M, Krausz F 2001 *Nature* **414** 509

[3] Lépine F, Ivanov M Y and Vrakking M J Raking 2014 *Nat. Photon.* **8** 195

[4] McPherson A, Gibson G, Jara H, Johann U, Luk T S, McIntyre I A, Boyer K and Rhodes C K 1987 *J. Opt. Soc. Am. B-Opt. Phys.* **4** 595

[5] Paul P M, Toma E S, Breger P, Mullot G, Auge F, Balcou P, Muller H G and Agostini P 2001 *Science* **292** 1689

[6] Popmintchev D, Hernandez-Garcia C, Dollar F, Mancuso C, Perez-Hernandez J A, Chen M C, Hankla A, Gao X H, Shim B, Gaeta A L, Tarazkar M, Romanov D A, Levis R J, Gaffney J A, Foord M, Libby S B, Jaron-Becker A, Becker A, Plaja L, Murnane M Playa, Kapteyn H C and Popmintchev T 2015 *Science* **350** 1225

[7] Popmintchev T, Chen M C, Popmintchev D, Arpin P, Brown S, Alisauskas S, Andriukaitis G, Balciunas T, Mucke O D, Pugzlys A, Baltuska A, Shim B, Schrauth S E, Gaeta A, Hernandez-Garcia C, Plaja L, Becker A, Jaron-Becker A, Murnane M Chauth and Kapteyn H C 2012 *Science* **336** 1287

[8] Ghimire S, DiChiara A D, Sistrunk E, Agostini P, DiMauro L F and Reis D A 2011 *Nat. Phys.* **7** 138

[9] Liu H Z, Li Y L, You Y S, Ghimire S, Heinz T F and Reis D A 2017 *Nat. Phys.* **13** 262

[10] Luu T Lou, Garg M, Kruchinin S Y, Moulet A, Hassan M T and Goulielmakis E 2015 *Nature* **521** 498

[11] Ndabashimiye G, Ghimire S, Wu M X, Browne D A, Schafer K J, Gaarde M B and Reis D A 2016 *Nature* **534** 520

[12] Schubert O, Hohenleutner M, Langer F, Urbanek B, Lange C, Huttner U, Golde D, Meier T, Kira M, Koch S W and Huber R 2014 *Nat. Photon.* **8** 119

[13] Vampa G, Hammond T J, Taucer M, Ding X, Ropagnol X, Ozaki T, Delprat S, Chaker M, Thire N, Schmidt B E, Legare F, Klug D There, Naumov A Y, Villeneuve D M, Staudte A and Corkum P B 2018 *Nat. Photon.* **12** 465

[14] Yoshikawa N, Tamaya T and Tanaka K 2017 *Science* **356** 736

[15] You Y S, Reis D A and Ghimire S 2017 *Nat. Phys.* **13** 345

[16] You Y S, Wu M X, Yin Y C, Chew A, Ren X M, Gholam-Mirzaei S, Browne D A, Chini M, Chang Z H, Schafer K J, Gaarde M B and Ghimire S 2017 *Opt. Lett.* **42** 1816

[17] You Y S, Yin Y, Wu Y, Chew A, Ren X, Zhuang F, Gholam-Mirzaei S, Chini M, Chang Z and Ghimire S 2017 *Nat. Commun.* **8** 724

[18] Du T Y, Huang X H and Bian X B 2018 *Phys. Rev. A* **97** 6

[19] Golde D, Meier T and Koch S W 2008 *Phys. Rev. B* **77** 6

[20] Jiang S C, Wei H, Chen J G, Yu C, Lu R F and Lin C D 2017 *Phys. Rev. A* **96** 11

[21] Li L, Lan P F, He L X, Cao W, Zhang Q B and Lu P X 2020 *Phys. Rev. Lett.* **124** 6

[22] Song X, Yang S, Zuo R, Meier T and Yang W 2020 *Phys. Rev. A* **101** 033410

[23] Vampa G, McDonald C R, Orlando G, Klug D Zou, Corkum P B and Brabec T 2014 *Phys. Rev. Lett.* **113** 073901

[24] Wu M X, Ghimire S, Reis D A, Schafer K J and Gaarde M B 2015 *Phys. Rev. A* **91** 11

[25] Yu C, Zhang X R, Jiang S C, Cao X, Yuan G L, Wu T, Bai L H and Lu R F 2016 *Phys. Rev. A* **94** 8

[26] Ghimire S, DiChiara A D, Sistrunk E, Szafruga U B, Agostini P, DiMauro L F and Reis D A 2011 *Phys. Rev. Lett.* **107** 167407

[27] Hohenleutner M, Langer F, Schubert O, Knorr M, Huttner U, Koch S W, Kira M and Huber R 2015 *Nature* **523** 572

[28] Taucer M, Hammond T J, Corkum P B, Vampa G, Couture C, Thire N, Schmidt B E, Legare F, Selvi H, Unsuree N, Hamilton B, Echtermeyer T J and Denecke M A 2017 *Phys. Rev. B* **96** 195420

[29] Luu T T and Worner H J 2018 *Nat. Commun.* **9** 6